Spray Characteristics of Prefilming Type of Airblast Atomizer

T. Inamura*, M. Shirota, M. Tsushima, M. Kato,
S. Hamajima and A. Sato
Faculty of Science and Technology, Hirosaki University, Hirosaki, Japan
tina@cc.hirosaki-u.ac.jp and mshirota@cc.hirosaki-u.ac.jp

Abstract

The spray characteristics of a prefilming type of airblast atomizer were experimentally investigated. Firstly, we observed the breakup phenomena at the wall edge of the liquid film flowing over the solid wall using the high-speed video movie. By the observation at the wall edge, the liquid film deforms into the bag-shaped sheet, which consists of a thin liquid film attached to a thick rim. The thin liquid film disintegrates into numerous fine droplets, and the thick ligaments attaching to the wall edge remain. Then the thick ligaments disintegrate into coarse droplets. The new numerical model of a film breakup at the wall edge was proposed. The new model assumes that the mean droplet diameter is determined by the coarse droplets generated by the breakup of a ligament attaching to the wall edge. So, concerning to the new breakup model, we focused on the ligament breakup. The numerically predicted wavelength, ligament diameter and mean droplet diameter were compared with the experiments. The predicted characteristics, such as wavelength, ligament diameter and mean droplet diameter, were almost coincident with the experiments except at low air velocity. The droplet mass flux was measured by the isokinetic probe. The droplet mass flux distributions are expressed by a normal distribution function which is normalized with a maximum flux at the center and half width at half maximum.

Introduction

The breakup phenomena of a liquid film flowing over a solid wall is usually observed in an automobile engine, jet engine, boiler combustor and general heat exchanger. In the recent jet engine the prefilming type of airblast atomizer has been used to meet the exhauset gas regulation because it has a good spray characteristics even at low fuel injection pressure. This type of atomizer utilizes the high-speed air stream flowing in the combustor for the atomization of a liquid fuel. So, the pressure loss of atomizing air in an atomizer is smaller than a conventional pneumatic atomizer utilizing atomizing air.

The atomization mechanism of a prefilming type of airblast atomizer is known as follows: The fuel is driven along the solid wall surface as a wavy film by the coflowing air stream, and then the liquid film is disintegrated at the wall edge by the air streams flowing on the both sides of the solid wall, the so-called prefilmer. Spray quality of a prefilming type of airblast atomizer is understood to be characterized by a liquid film thickness, liquid flowrate and air velocity. Rizk and Lefebvre[1] investigated the spray characteristics of this type of atomizer, and concluded that a liquid film thickness is an important parameter for spray characteristics. Many other researchers have been investigated the spray characteristics of a prefilming type of airblast atomizer, and proposed the empirical equations of mean droplet size[2,3,4].

On the other hand, the numerical simulation has been utilized recently for the design of a combustor to save a time and cost required for experiments[5,6]. Due to the rapid development of a computer performance, the numerical simulation of a spray flow and combustion process in the combustor has been possible. At this stage the liquid breakup model in an atomization process is necessary for the numerical simulation[7].

This study aims to clarify the spray characteristics of a prefilming type of airblast atomizer and to make a numerical model of a film breakup to predict the spray characteristics of this type of atomizer, and finally to compare the numerically predicted spray characteristics with the measurements. To put it concretely, as the first step, the liquid film behaviors on the prefilmer and at the prefilmer edge were experimentally investigated. Then, the numerical breakup model of a liquid film at the prefilmer edge was proposed. Finally, the numerical predictions of the wavelength, ligament diameter and mean droplet diameter were compared with the measurements.

Experimental Apparatus

Figure 1 shows the experimental apparatus. The air generated by the blower is supplied to the contraction nozzle via a honeycomb. The exit of a contraction nozzle is rectangular with the width of 50mm and the height of 30mm. The test atomizer is attached to the exit of the contraction nozzle. The water in the pressure tank is

* Corresponding author: tina@cc.hirosaki-u.ac.jp

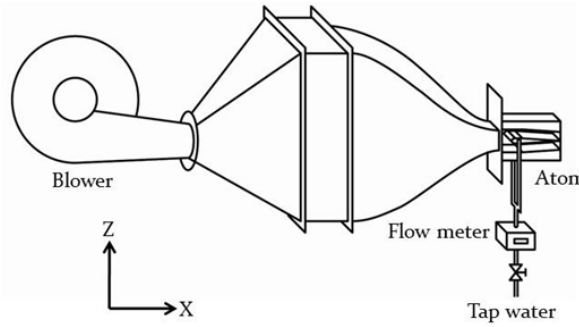

Figure 1 Experimental apparatus.

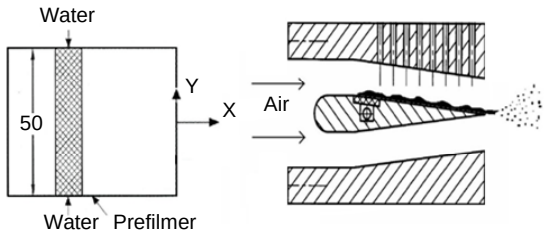

Figure 2 Test atomizer.

pressurized by a high-pressure air from the compressor, and then it is supplied to the prefilmer in the test atomizer through a flow meter.

Figure 2 shows the test atomizer used in the present study. The test atomizer is two-dimensional for easy observation of liquid disintegration phenomena. The prefilmer is set at the center in the atomizer, and in order to uniform the liquid flowrate distribution in the traverse direction the porous metal was used at a liquid exit part. For the optical access, the upper and side parts were made of the acrylic plastic. The X-coordinate is in the flow direction, Y-coordinate is in the traverse direction, and Z-coordinate is perpendicular to the prefilmer. The coordinate system is the right-handed system. The origin was set at the center of a prefilmer edge. The disintegration phenomena of a liquid film at the prefilmer edge were observed by the instantaneous digital camera and the high-speed video camera. The wavelength of the surface wave of a liquid film on the prefilmer was measured by the image processing method, that is two-dimensional Fast Fourier Transform (FFT), using instantaneous photographs. And the thickness of a liquid film flowing over a prefilmer was measured by the contact needle probe. The droplet mass flux was measured by the isokinetic probe. And the droplet size was measured by the Fraunhofer diffraction method. The details of the experimental apparatus are presented in the previous paper[8].

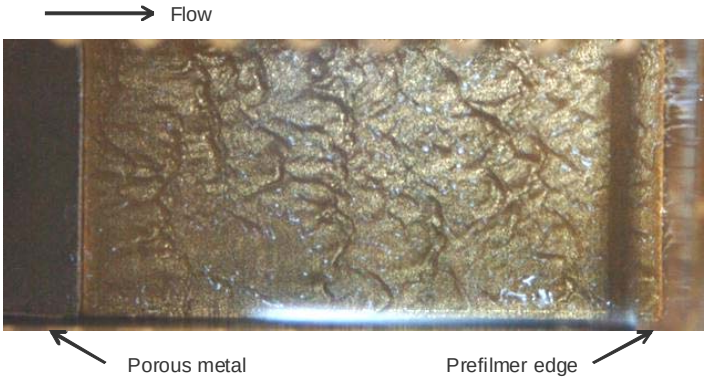

Figure 3 Surface waves.

In the present study, tap water was used as the atomized liquid and air as the atomizing gas. The liquid volume flowrate per unit width of a prefilmer was ranged from 0.8 to 3.2cm^3/(s cm), and the gas velocity at the atomizer exit was ranged from 17 to 76.5m/s.

Liquid Film Breakup Phenomena

Figure 3 shows the surface waves on the liquid film surface flowing over the prefilmer under the air velocity of 51m/s and liquid flowrate of 2.0cm^3/(s cm). The air and liquid flow from left to right in photographs. The three-dimensional scaly waves appear on the liquid film surface. The liquid film is thick at the rim of a scaly wave. The thick rim of a scaly wave becomes a thick rim at the periphery of a bag-shaped liquid film when it arrives at the edge of the prefilmer.

Figure 4 shows the effect of a liquid flowrate and air velocity on the liquid film breakup phenomena at a prefilmer edge. The air and liquid flow from bottom to top in the photographs. As the air velocity increases the breakup length of a liquid film shortens, and finer droplets are generated. The diameter of a ligament attaching to the prefilmer edge gets thin and the space between ligaments in the traverse direction narrows as the air velocity increases. As the liquid flowrate increases the breakup length increases and coarser droplets are generated.

Figure 5 shows the details of the bag-type breakup phenomena at the prefilmer edge. As shown in Fig.3 the wave consists of thin liquid film and thick rim at the periphery of liquid film. The liquid film is bulged out the thin liquid sheet downward by an air stream at the prefilmer edge. The thin, bag-shaped liquid film has a thick rim at periphery. The fine droplets are generated by the disintegration of a thin, bag-shaped liquid film, and the thick ligaments remain attaching to the prefilmer edge. Then the thick ligament disintegrates and the coarse droplets are generated.

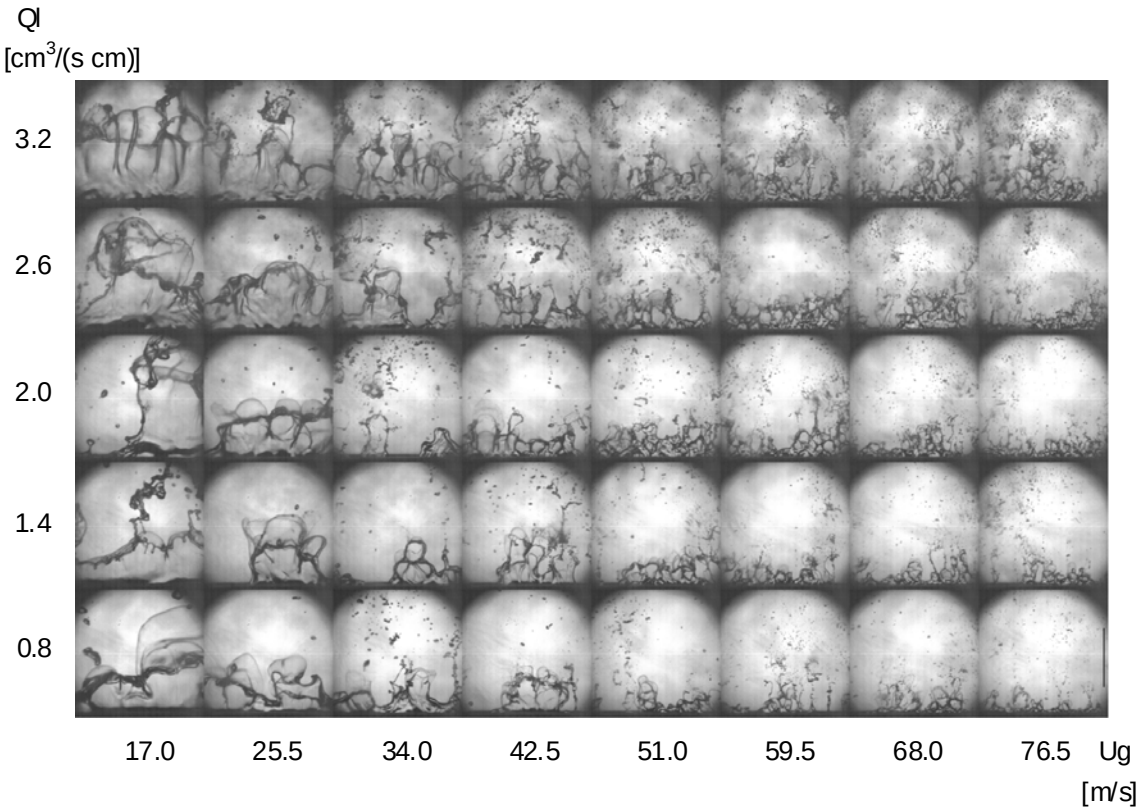

Figure 4 Liquid film breakup phenomena.

Liquid Film Breakup Model

The experiments consume much time and cost. The numerical analysis is expected to save those. There are many researches to analyze numerically the spray flow and combustion in the combustor. However, the numerical simulation of the spray formation is very difficult because the liquid disintegration phenomena are very complicated. The phenomena are small size, high-speed and unsteady. So, in the present stage it seems to be the better way to use the liquid breakup model instead of the direct simulation of the liquid disintegration.

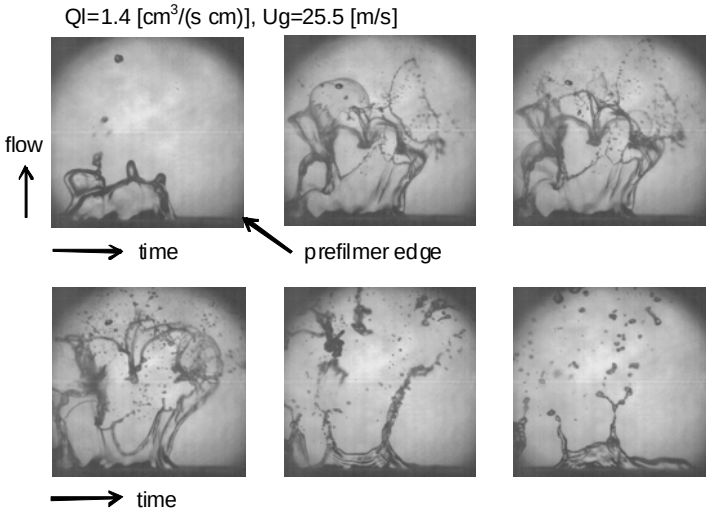

Figure 5 Ligaments formation mechanism.

Firstly, we analyzed the liquid film flow on the prefilmer to predict the wavelength on the liquid film surface. Waves in the liquid flow direction are assumed to be generated according to the Kelvin-Helmholtz instability. The wavelength in the liquid flow direction, λ_1 is expressed as follows[9];

$$\lambda_1 = C\delta_\omega \sqrt{\frac{\rho_l}{\rho_g}} \tag{1}$$

where C indicates a correction factor which equals to 1.6 in the present study, δ_ω a thickness of the eddy boundary layer, and ρ the density. Subscripts l and g indicate the liquid and gas, respectively. The thickness of the eddy boundary layer is expressed by the following equation[9];

$$\delta_\omega = 3.56\frac{H_g}{\sqrt{\mathrm{Re}_{Hg}}} \tag{2}$$

where H_g indicates the width of a gas flow channel which equals to 10mm in the present study. The Re_{Hg} indicates the gas Reynolds number which is expressed as follows;

$$\mathrm{Re}_{Hg} = \frac{\rho_g U_g H_g}{\mu_g} \tag{3}$$

where U_g indicates the gas velocity at the atomizer inlet, and μ indicates the viscosity.

Waves in the traverse direction are assumed to be generated according to the Rayleigh-Taylor instability. The wavelength in the traverse direction, λ_2 is expressed as follows[9];

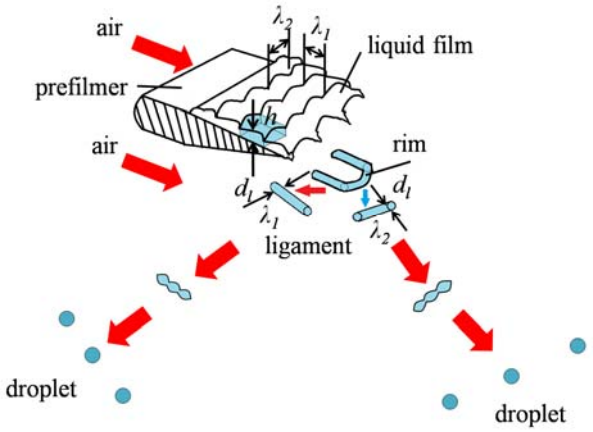

Figure 6 Breakup model.

$$\lambda_2 = 2\pi\sqrt{\frac{6BC}{C_d}}\delta_\omega\left(\frac{\rho_l}{\rho_g}\right)^{1/4}\sqrt{\frac{\sigma}{\rho_g\left(U_g - U_l\right)^2\delta_\omega}} \tag{4}$$

where B indicates a correction factor which equals to 0.25 and C_d indicates the drag coefficient which equals to 2.01 in the present study. The σ indicates the surface tension. The U_l indicates the liquid mean velocity at the prefilmer edge which was calculated by the liquid flowrate as follows;

$$U_l = \frac{Q_l}{h} \tag{5}$$

where Q_l indicates the liquid volume flowrate per unit width and h indicates the mean liquid film thickness measured at the prefilmer edge by the contact needle probe.

Secondly, we proposed the new breakup model of a liquid film at the prefilmer edge. To predict the mean droplet size we neglected the fine droplets generated by the disintegration of a thin liquid film bulged by the air stream like a bag, because the contributions of fine droplets to the mean droplet size are small. We know the importance of fine droplets for other aspects of the spray. As the first step, we determined to neglect fine droplets for the simplification of the breakup model. So, we focused on the thick ligaments attaching to the prefilmer edge generated by the disintegration of a bag-shaped sheet. Figure 6 shows the breakup model of a liquid film proposed in the present study. The thick rim consists of two straight cylinders and a half ring of which the diameter equals to the wavelength in Y-direction. The diameter of a cylinder, d_l can be calculated from the mass conservation as follows;

$$d_l = 2\sqrt{\frac{\lambda_1\lambda_2 h}{\pi\left(2\lambda_1 + \frac{\pi}{2}\lambda_2\right)}} \tag{6}$$

The cylinder is disintegrated into coarse droplets according to the Weber's theory. The mean droplet size, d_D is expressed as follows[10];

$$d_D = 1.88 d_l \left(1 + 3Oh\right)^{1/6} \tag{7}$$

where Oh indicates the Ohnesorge number which is expressed as follows;

$$Oh = \frac{\mu_l}{\sqrt{\rho_l \sigma d_l}} \tag{8}$$

By the investigation on the ligament disintegration from Marmottant et al., the droplet size distribution is expressed as following Gamma function[11];

$$P_B(x = D/<D>) = \frac{n^n}{\Gamma(n)} x^{n-1} e^{-nx} \qquad (9)$$

where P_B indicates the probability distribution function and <D> indicates the mean droplet size. Γ(n) indicates the Gamma function and n is constant between 2 and 4. In the present study, we substitute d_D obtained by Eq.(7) for <D> in Eq.(9) and put n=4. Around four thousands droplets were generated according to the droplet size distribution expressed by Eq.(9). Figure 7 shows the droplet size distribution at U_g=51m/s and Q_l=2.0cm^3/(s cm). In this case, the liquid film thickness is 181μm, ligament diameter is 466μm, and <D>=878μm. The horizontal axis in the figure, D indicates the droplet size and vertical axis, N indicates the number of generated droplet. The droplet size distribution corresponds to the Nukiyama-Tanasawa distribution with α=3 and β=1.

The coarse droplets may be disintegrated again into fine droplets. We considered the secondary breakup of a coarse droplet using the TAB model[12].

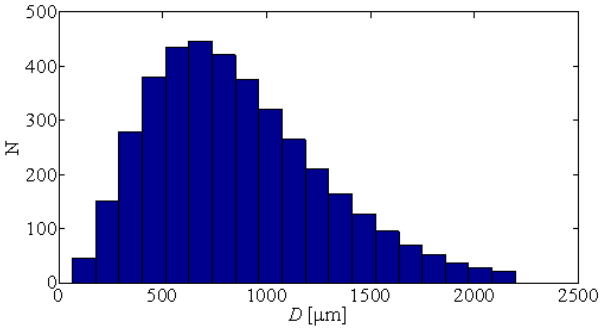

Figure 7 Size distribution of generated droplets.

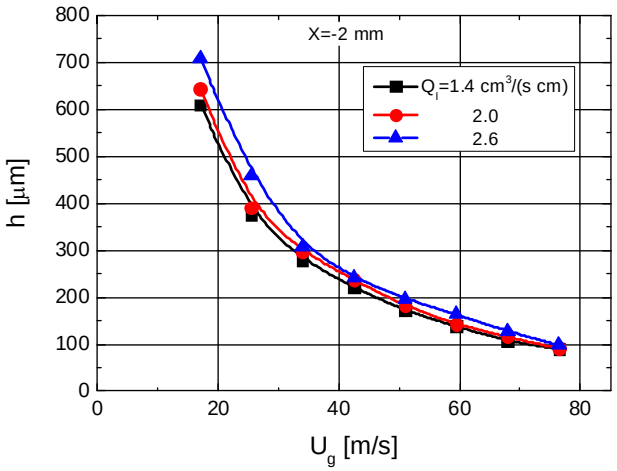

Figure 8 Liquid film thickness.

Results and Discussions

Liquid film thickness is one of the important parameters which determine the spray characteristics. Figure 8 shows the mean liquid film thickness measured by the contact needle probe at the prefilmer edge. Measurement point is 2mm upstream from the prefilmer edge. The film thickness decreases as the air velocity increases. At low air velocity the film thickness increases with the liquid flowrate. However, at high air velocity the effect of the liquid flowrate on the film thickness becomes small.

Figures 9 and 10 show the predicted wavelengths compared with the measurements. Figure 9 shows the wavelength in the liquid flow direction. The wavelength decreases slightly as the air velocity increases. The influence of the liquid flowrate on the wavelength is small. The predicted wavelengths are almost coincident with measurements except at low air velocity. At U_g=34.0m/s, the model shows smaller wavelengths than measurements, especially at large liquid flowrate. Since the measurement data used for the wavelength measurement at low air velocity are few, the reliability of the measurements of the wavelength at low air velocity is relatively lower than those at other air velocity conditions. Figure 10 shows the wavelength in the traverse direction. The wavelength decreases as the air velocity increases. The influence of the air velocity on the wavelength is larger than the wavelength in the liquid flow direction. The influence of the liquid flowrate on the wavelength is small. The predicted wavelengths show good agreements with the measurements.

Figure 11 shows the predicted ligament diameters compared with the measurements with error bars. As the air velocity increases the ligament diameter decreases. The ligament diameter increases as the liquid flowrate increases. Since the measurements of ligament diameter scatter widely, the quantitative comparisons of ligament diameter between the measurements and predictions are difficult. The predicted ligament diameters show good qualitative agreements with the measurements. However, in the case of calculations the influences of the liquid flowrate on the ligament diameter are smaller than the measurements.

Figures 12, 13 and 14 show the predicted Sauter mean diameters (SMDs) with the measurements at three distances from the prefilmer edge. The liquid flowrates of Figs.12, 13 and 14 are 1.4, 2.0 and 2.6 cm^3/(s cm), respectively. Regardless of the liquid flowrate, the SMD decreases monotonously as the air velocity increases. The influences of the distance from the prefilmer edge on the SMD are small except at low air velocity. At low air velocity the SMD decreases slightly according to the distance from the prefilmer edge. This is due to the secondary breakup of coarse droplets. At low air velocity, since the breakup time required for secondary breakup is large by comparison with that at high air velocity a coarse droplet travels long distance until it disintegrates

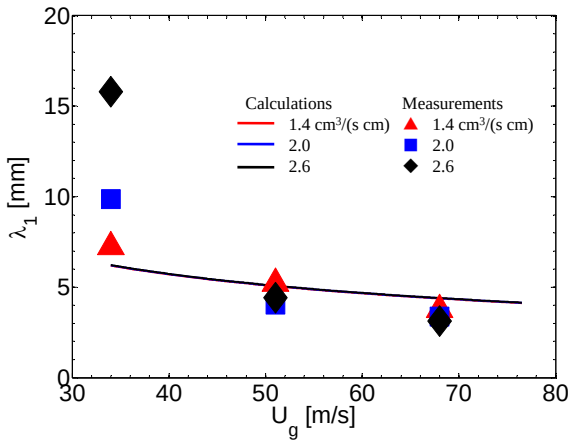

Figure 9 Wavelength in liquid flow direction.

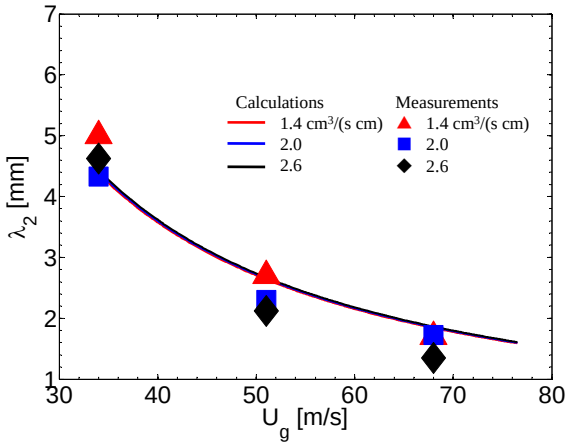

Figure 10 Wavelength in traverse direction.

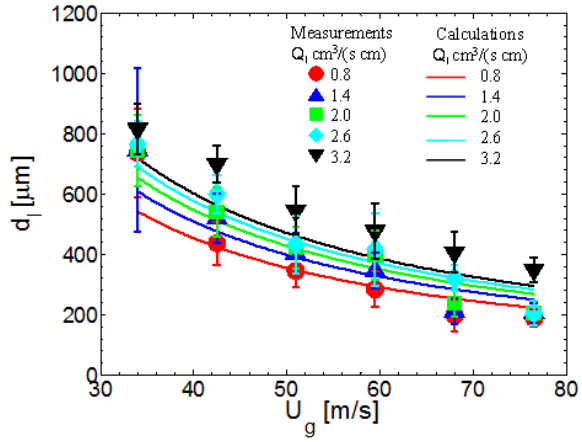

Figure 11 Ligament diameter.

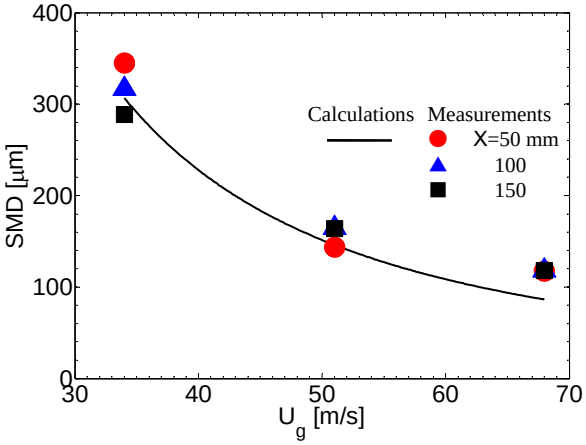

Figure 12 Comparisons of SMD (Q_l=1.4cm^3/(s cm).

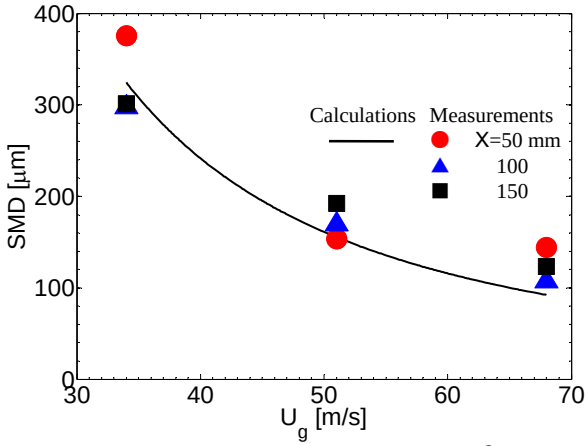

Figure 13 Comparisons of SMD (Q_l=2.0cm^3/(s cm).

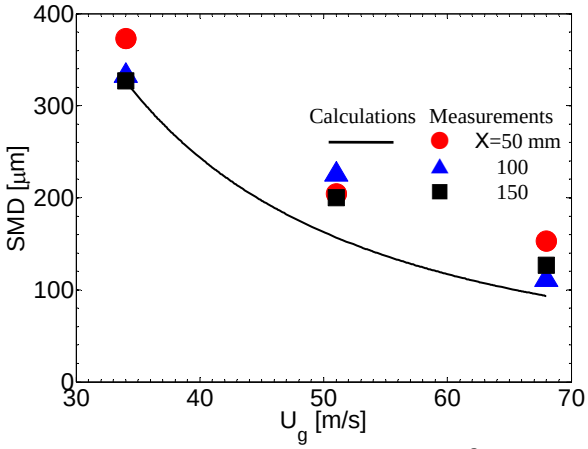

Figure 14 Comparisons of SMD (Q_l=2.6cm^3/(s cm).

again. On the other hand, in the case of calculation the distance from the prefilmer edge has no influence on the SMD. This is because the calculated breakup time in the TAB model is so short that secondary breakup completes in the vicinity of the prefilmer edge. So, in the case of calculations no influence of the distance on the SMD appears in the graph. In the calculations the breakup time of TAB model should be estimated more exactly. The predicted SMDs show good agreements with the measurements in Figs.12 and 13. In Fig.14 the predicted SMDs show smaller values than the measurements. At large liquid flowrate, since the droplet number density is large the coalescence between droplets may occur. In the present model calculation the coalescence between droplets is not taken account.

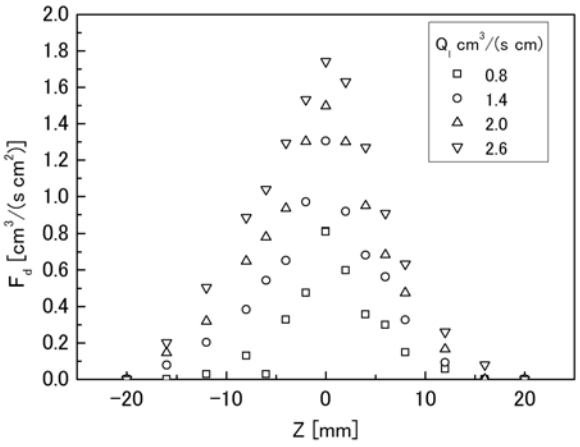

Figure 15 Droplet mass flux distribution.

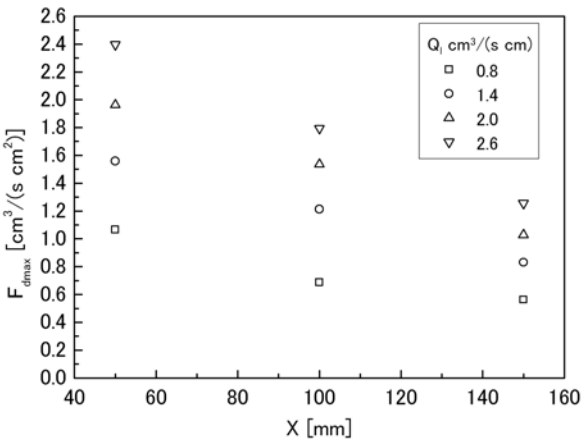

Figure 16 Maximum droplet mass flux.

Figure 15 shows the droplet mass flux distribution in the Z-direction at X=50mm. The droplet mass flux was measured by the isokinetic probe at U_g=51m/s. The distribution shows the shape of a normal function. As the liquid flowrate increases the distribution becomes broad and the maximum mass flux on the center axis increases.

Figure 16 shows the influence of the downward distance from the prefilmer edge on the droplet mass flux on the center axis measured by isokinetic probe at U_g=68m/s. As the measurement point goes downstream the mass flux decreases. As the liquid flowrate increases the mass flux increases throughout the distances from the prefilmer edge.

Figure 17 shows the non-dimensional distribution of droplet mass flux in the Z-direction. The horizontal axis is normalized by the half width at half maximum and the vertical axis is normalized by the droplet mass flux on the center axis. The mass flux was measured at the various downward distances from the prefilmer edge. The droplet mass flux distribution from the coaxial airblast atomizer can be expressed by the normal distribution function[15]. In the case of a coaxial airblast atomizer, the distribution is axisymmetric. In the present study, since the atomizer is two-dimensional the distribution is expected to be two-dimensional. So, we assumed the following normal distribution function for the droplet mass flux distribution[16];

$$\frac{F_d(X,0,Z)}{F_d(X,0,0)} = \exp\left[A\left(\frac{Z}{Z_{1/2}} \right)^2 \right] \qquad (10)$$

where F_d indicates the droplet mass flux and $Z_{1/2}$ means the half width at half maximum of the mass flux distribution. Since the droplet mass flux on the center axis is maximum, the F_d (X,0,0) in Eq.(10) equals to F_{dmax} in Figs.16 and 17. The constant, A in Eq.(10) indicates a correction factor which is determined by the comparison with the measurements. By the least square method of the measured mass flux, we obtained that A equals to -0.693. The solid line in the figure shows the empirical equation expressed by Eq.(10). The predicted mass flux distribution by Eq.(10) agrees well with the measurements.

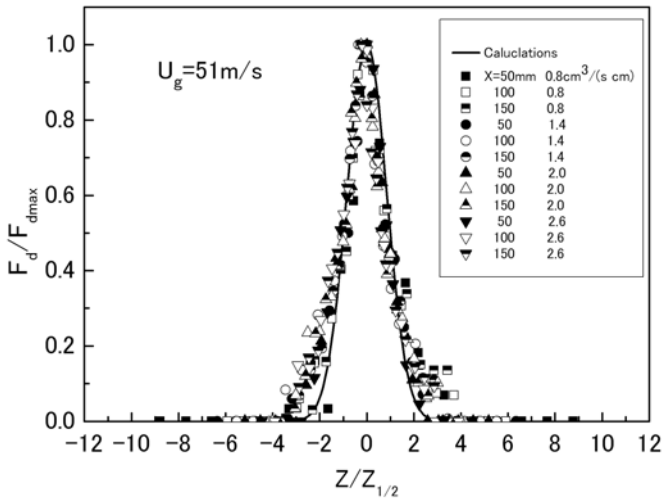

Figure 17 Non-dimensional droplet mass flux distribution.

Summary and Conclusions

The spray characteristics of a prefilming type of airblast atomizer were experimentally investigated using the two-dimensional test atomizer with a rectangular cross-section. New breakup model of a liquid film at a prefilmer edge was proposed from the observation of disintegration phenomena of a liquid film. And the predicted wavelengths, ligament diameter, and mean droplet diameter were compared with the measurements. The droplet mass flux distributions were measured by an isokinetic probe, and the distribution function for the droplet mass flux distribution was proposed using the normal distribution function. Consequently, the following results were obtained;

(1) At the prefilmer edge, liquid film is bulged out the thin liquid sheet with the thick rim at periphery. The fine droplets are generated by the disintegration of a thin liquid film, and the coarse droplets are generated by the disintegration of a thick rim.
(2) The new breakup model of a liquid film was proposed based on the Kelvin-Helmholtz and Rayleigh-Taylor instability. The new breakup model focuses on the disintegration of a thick rim and eliminates the disintegration of a thin, bag-shaped sheet.
(3) The new breakup model predicts well the wavelength in the flow and traverse directions except at low air velocity.
(4) The ligament diameter decreases as air velocity increases and liquid flowrate decreases. In the calculations by new breakup model, the effect of liquid flowrate on the ligament diameter is smaller than the measurements.
(5) At small liquid flowate the predicted SMDs show good agreements with the measurements. At large liquid flowrate the predicted SMDs show slightly smaller values than the measurements.
(6) The droplet mass flux distribution is expressed by the following empirical equation;

$$\frac{F_d(X,0,Z)}{F_d(X,0,0)} = \exp\left[-0.693\left(\frac{Z}{Z_{1/2}}\right)^2\right]$$

References

[1] Rizk, N. K. and Lefebvre, A. H., *Transactions of the ASME* 102: 706-710 (1980).
[2] Rizk, N. K. and Lefebvre, A. H., *AIAA Journal* 21: 1139-1142 (1983).
[3] Sattlemayer, T. and Wittig, S., *Transactions of the ASME* 108: 465-472 (1986).
[4] Aigner, M. and Wittig, S., *Transactions of the ASME* 110: 105-110 (1988).
[5] Shi, J. –M., Wenzlawski, K., Helie, J., Nuglisch, H. and Cousin, J., *23rd European Conference on Liquid Atomization and Spray Systems*, Brno, Czech Republic, September 6-8, 2010.
[6] Kim, T, Kim, Y. and Kim, S. –K., *14th Annual Conference on Liquid Atomization and Spray Systems –Asia*, Jeju, Korea, October 21-22, 2010.
[7] Inamura, T., Yanaoka, H. and Tomoda, T., *AIAA Journal* 42: 614-621 (2004).
[8] Tsushima, M., Yamashita, K., Sato, A., Inamura, T. and Shirota, M., *18th Symposium (ILASS-Japan) on Atomization*, Fukuoka, Japan, December 17-18, 2009 (in Japanese).
[9] Boukra, M., Cartellier, A., Ducasse, E., Gajan, P., Lalo, M., Noel, T. and Strzelecki, A., Comptes Rendus Mecanique 337: 492-503 (2009).
[10] Dombrowski, N. and Johns, W. R., *Chemical Engineering Sciences* 18: 203-214 (1963).
[11] Marmottant, P. and Villermaux, E., *Journal of Fluid Mechanics* 498: 73-111 (2004).
[12] O'Rourke, P. J. and Amsden, A. A., *SAE Technical Paper* 872089 (1987).